Cost-effective PROton Exchange MEmbrane WaTer Electrolyser for Efficient and Sustainable Power-to-H2 Technology

Grant No. 862253

***Start date**: 01.04.2020 – **Duration**: 36 months*
***Project Coordinator**: Daniel García-Sánchez - DLR*

D1.6: Summary report on materials developed: updated information on upscaling.

WP1 Catalyst Development

WP *Leader*: *CENmat*
Deliverable Responsible: *CENmat*
Deliverable Author(s): Sambal S Ambu, (CENmat), S Siracusano, F.Giacobello, A.Arico (CNR), Maria Retuerto (CISC)

Status: F
(D: Draft, FD: Final Draft, F: Final)
Dissemination level: PU
(PU: Public, CO: Confidential,
only for Consortium members (including the Commission Services))

This project has received funding from the European Union's Horizon 2020 research and innovation programme under grant agreement No 862253

This project has received funding from the European Union's Horizon 2020 research and innovation programme under grant agreement No 862253.

Document history

Version Number	Date of issue	Author(s)	Brief description of changes
V 1	06/07/2023	S Siracusano, F.Giacobello,A.Arico (CNR)	Creation of CNR report
V2	18/07/2023	Sambal Ambu (CENmat)	Creation of CENmat report
V3	19/07/2023	Maria Retuerto (CISC)	Creation of CSIC report
V4	26/07/2023	Sambal Ambu	Creation of consolidated report

Contents

List of Figures

List of Tables

Acronyms

ACL – Anode catalyst layer
BET - Brunauer Emmett-Teller
CRM – Critical raw material
CV - Cyclic Voltammetry
ECSA- Electro chemical surface area
EDX- Energy-dispersive X-ray
EIS- Electrochemical Impedance Spectroscopy
HER- Hydrogen Evolution Reaction
ICP- Inductively Coupled Plasma
LSV-Linear sweep voltammetry
MEA- Membrane electrode assembly
OER- Oxygen Evolution Reaction
OCP- Open circuit potential
PEM- Proton Exchange Membrane
PEMWE- Proton exchange membrane water electrolysis
RDE -Rotating Disk Electrode
RHE- Reversible Hydrogen Electrode
SEM- Scanning Electron Microscopy
TEM -Transition Electron Microscopy
XPS- X-ray Photoelectron Spectroscopy
XRD- X-ray Diffraction
XRF – X-Ray fluorescence spectroscopy
WE - Working Electrode

1 CRM reduced catalysts

1.1 Oxygen Evolution reaction (OER)

In this last part of the Proyecto *CSIC* partner has prepared mixed oxides with reduced content of Ru. *CSIC* has chosen one of those mixed oxides to be tested in PEMWE:

$NdMn_{1.5}Ru_{0.5}O_5$

By designing this catalyst *CSIC* discovered a novel crystal structure that has been never reported as active for the oxygen reactions. *CSIC* has proven very high OER activity of this oxide in acid media with low overpotential and high mass activity, and also very promising durability.

R_2NiRuO_6

By designing this catalyst *CSIC* is exploring the family of Ru perovskites as possible OER catalysts. The Ru perovskites tested before had never achieved good values of durability, so dissolving during the first cycles of reaction. In contrast, R_2NiRuO_6 and in particular Dy_2NiRuO_6 shows a durability of more than 5000 OER cycles, and even after so many cycles the perovskite structure is maintained in the bulk catalyst, only with a surface restructuration.

1.1.1 Synthesis and Characterization: CSIC

$NdMn_{1.5}Ru_{0.5}O_5$ and R_2NiRuO_6 were synthesized by the citrates method. In all the cases, the stoichiometric amounts of the starting materials were dissolved in 100 mL of a citric acid solution 0.52 M with 5 mL of HNO_3 (Alfa Aesar, 68-70%) under vigorous magnetic stirring. Then, the suspension was evaporated at ca. 100 ºC leading to an organic resin in which cations are homogenously distributed. Subsequently, the mixture was dried at 140 ºC and thermally treated under static air in a horizontal furnace at 600 ºC (heating ramp of 2 ºC/min) and 800 ºC (heating ramp of 1.67 ºC/min) for 12 and 2 h, respectively. Finally, $NdMn_{1.5}Ru_{0.5}O_5$ precursors were further annealed at 800 ºC for 12 h in air. R_2NiRuO_6 perovskites with R= Dy and Tb were treated at 1100°C/12 h + 1100°C/12 h to obtain the pure samples, Nd and Pr needed only 1100°C/12 h, and Er, Ho and Y needed 1300°C/12 h.

The crystal structure of the catalysts was analyzed with a X-ray polycrystal PANalytical X´Pert PRO using nickel-filtered CuKα (1.541874 Å) radiation, with a 0.04º step size and accumulating 20 s per point. The refinement of the crystal structures was performed using the Rietveld method and the Fullprof crystallographic program.

Figure 1a shows the Rietveld refinement of the crystal structure of $NdMn_{1.5}Ru_{0.5}O_5$. The inset of the Figure depicts the schematic view of its crystal structure. The material is isostructural with $DyMn_2O_5$ (space group P*bam*). It contains infinite chains of $(Mn,Ru)^{4+}O_6$ octahedra sharing edges, and linked together by dimeric $(Mn)^{3+}O_5$ and NdO_8 units. The contraction of the *c* axis along with the short Ru/Mn-Ru/Mn distances of 2.60 Å between the $(Mn,Ru)^{4+}O_6$ octahedra suggest the presence of Ru/Mn-Ru/Mn metal bonding, since Ru-Ru in metallic Ru is 2.642 Å and Mn-Mn in metallic Mn are 2.34 Å.[1,2] Note that the

distance of 2.60 Å is in good agreement with the distances previously reported in $NdMn_{1.5}Ru_{0.5}O_5$ from Neutron Powder Diffraction data [3].

Figure 1b shows the XRD patterns of the perovskites R_2NiRuO_6 (R= Er, Ho, Y, Dy, Tb, Nd). The crystal structures can be defined in the monoclinic $P2_1/n$ space group, with long-range ordering of Ni^{2+} and Ru^{4+} at the octahedral B positions of the perovskite. The unit-cell parameters and volumes increase as the ionic radii of the rare earth in the A site of the perovskite increases in a pseudo-eightfold coordination environment, in the $Er^{3+}<Y^{3+}\leq Ho^{3+}<Dy^{3+}<Tb^{3+}<Nd^{3+}<Pr^{3+}$ order.[4]

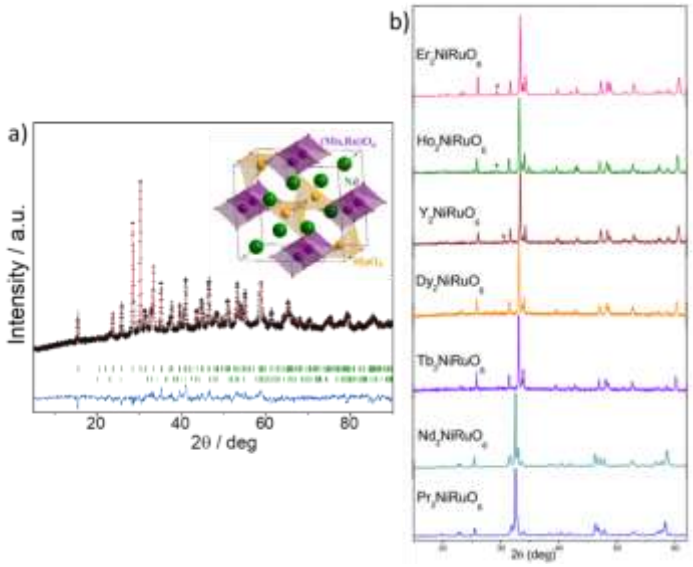

Figure 1 XRD of (a) $NdMn_{1.5}Ru_{0.5}O_5$ and (b) R_2NiRuO_6 catalysts.

Electrochemical Characterization Study: Catalytic Performance

The OER performance of the catalysts was first measured in acidic electrolyte using a rotating disk electrode (RDE). Experiments were performed using a three-electrode cell using an Ag/AgCl (3M) and a graphite rod as reference and counter electrodes, respectively. The reference electrode was calibrated by recording the hydrogen evolution reaction in an H_2-saturated 0.1 M $HClO_4$ electrolyte using a Pt wire as the working electrode. The electrolyte, 0.1 M $HClO_4$, was prepared with $HClO_4$ (Sigma Aldrich; 70%) and MilliQ water (18.2 MΩcm). An Autolab PGSTAT320N potentiostat/galvanostat controlled by the NOVA 2.1 software was used. Potentials, reported vs the reversible hydrogen electrode (RHE), are *i*R corrected with the resistance value of 24 Ω measured by electrical impedance spectroscopy (EIS) at open circuit voltage in 0.1 M $HClO_4$.The electrocatalyst was deposited on a RDE (Pine Instruments), with a glassy carbon disk electrode of 5 mm outer diameter. Before catalyst deposition, the electrode was polished with alumina slurry (0.05 μm, PINE) to a mirror ending, and rinsed with triply distilled water. Each catalyst was deposited onto the electrode by means of an ink, which was prepared by dispersing 5 mg of catalyst and 1 mg of carbon black Vulcan-XC-72R into 970 μL tetrahydrofuran (THF) and 30 μL of Nafion 117 solution (5%) with an Ultrasonic mixer UP50H (Hielscher). The catalyst loading on the electrode was 0.255 mg cm^{-2}. The OER polarization curves were obtained by recording cyclic

voltammograms between 1.2 and 1.7 V vs RHE in O_2-saturated electrolyte at 10 mVs^{-1} and 1600 rpm. The durability was tested by consecutive cycling in the same range of potential.

OER Activity

The OER catalytic activity was measured in 0.1 M $HClO_4$ by cyclic voltammetry (CV) between 1.2 and 1.7 V vs. RHE, at 10 and 100 mV/s. Several measurements with different batches of catalysts have been performed to assess the reproducibility of the measurements.

$NdMn_{1.5}$ $Ru_{0.5}O_5$

Figure 2a shows the polarization curve for the OER with $NdMn_{1.5}Ru_{0.5}O_5$. The potential needed to reach 10 mA cm^{-2} is usually taken to benchmark the OER activity of electrocatalysts [5]. $NdMn_{1.5}Ru_{0.5}O_5$ records 1.5 V at such current, hence being among the most active Ru and Ir electrocatalysts reported in the literature, only outperformed by $SrRuO_3$-based catalysts and $CaCu_3Ru_4O_{12}$, respectively [6–8]. A Tafel slope of 45 mV dec^{-1} is calculated for $NdMn_{1.5}Ru_{0.5}O_5$ between 1.35 - 1.45 V. This value is very similar to the values typically reported for Ru catalysts, with Tafel slopes ranging between 40 and 60 mV dec^{-1}. Note that Ru Tafel slopes are lower than Ir ones, indicating that the OER is faster on Ru-based electrocatalysts.

Figure 2b shows the Ru-mass-normalized activity (i_M) of $NdMn_{1.5}Ru_{0.5}O_5$ for the OER, reaching a i_M of 525 A g_{Ru}^{-1} at 1.55 V. This i_M is among the highest ones in the literature, only behind $Y_2[Ru_{1.6}Y_{0.4}]O_{7-\delta}$ (~ 700 A g_{Ru}^{-1}), $Y_{1.7}Sr_{0.3}Ru_2O_7$ (1018 A g_{Ru}^{-1}) and $CaCu_3Ru_4O_{12}$ (1942 A g_{Ru}^{-1}) [8–10]. Note that Ru based pyrochlores and perovskites have been reported active for the OER. However, this is the first time that a Ru oxide with a crystal structure from the $DyMn_2O_5$ family is reported to display OER activity.

R_2NiRuO_6

Figure 2c illustrates the 30th OER cycle for all R_2NiRuO_6. The catalysts suffer from surface reconstruction during the first 20-30 cycles so the best activity is achieved after 30 OER cycles, where the activity stabilizes. This reconstruction has been previously observed in Ru mixed oxides and it has been ascribed to the Ru-enrichment of the surface during the first cycles.[11,12] Therefore, after 30 cycles, we determined the potential to reach a current density of j= 10 mA cm^{-2}_{geom}. The catalyst exhibiting the highest activity is Dy_2NiRuO_6, reaching a potential of 1.507 V @ 10 mA cm^{-2}_{geom}. The following best catalyst among the studied ones is Y perovskite with ca. 1.6 V @ 10 mA cm^{-2}_{geom}. Dy_2NiRuO_6 presents a low potential, very similar to the best reported catalysts,[6–8,13–15] which are mainly based in doped simple oxides and perovskites. Note that the stability of perovskites is usually very low[6,7]

Figure 2d shows the Ru mass-specific activity of Dy_2NiRuO_6, recording 660 A g^{-1}_{Ru} at 1.55 V. This mass activity is similar to the one reported for Y_2MnRuO_7, and larger than that of $Y_2Ru_2O_7$ (300 A g^{-1}_{Ru} at 1.55 V).[11,12]

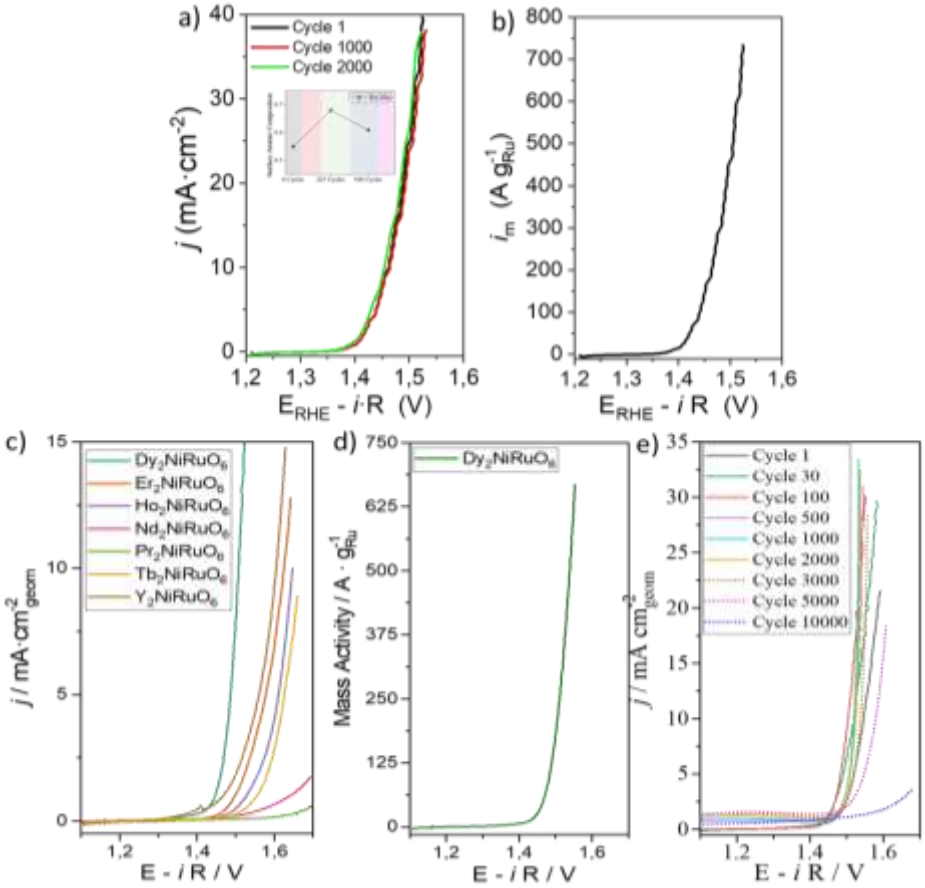

Figure 2 (a) Polarization curve for $NdMn_{1.5}Ru_{0.5}O_5$ in 0.1 M $HClO_4$. (b) Ru mass activity for $NdMn_{1.5}Ru_{0.5}O_5$. (c) Polarization curve for R_2NiRuO_6 in 0.1 M $HClO_4$. (d) Ru mass activity for R_2NiRuO_6. (e) Polarization curve for Dy_2NiRuO_6 in 0.1 M HClO4 and the evolution of the catalytic response with cycling

OER Durability

$NdMn_{1.5}Ru_{0.5}O_5$

The durability of $NdMn_{1.5}Ru_{0.5}O_5$ during the OER has been evaluated by recording consecutive cyclic voltammograms between 1.1 and 1.7 V at 100 mV s^{-1}. As shown in Figure 2a, the OER activity of the oxide remains stable during 2000 cycles. A closer inspection of the polarization curves reveals a slight improvement of the initial activity during the first 200 cycles (ΔE -10 mV). After 2000 cycles, the loss of the OER activity starts. However, after 5000 cycles 70% of the Ru mass-normalized activity is still maintained.

R_2NiRuO_6

Durability tests on R_2NiRuO_6 have been performed, by OER cycling between 1.1 and 1.7 V at 100 mV·s^{-1}. Figure 2e shows the loss of activity for Dy_2NiRuO_6 after 3000 cycles. Dy_2NiRuO_6 is the most active and durable catalyst, followed by Y, Er, Ho, Tb and, finally Nd and Pr that are very unstable. For instance,

Y_2NiRuO_6 activity lasts for 500 CVs, Er_2NiRuO_6 losses 28 % of its activity after 60 cycles, Ho_2NiRuO_6 losses 26% after 30 cycles and Tb_2NiRuO_6 loses 46 % after 30 CVs. This result indicates that the crystallographic parameters that have an effect over the catalytic activity also affect the durability/stability.
In the first OER cycle for Dy_2NiRuO_6 the catalyst achieves approximately 15 mA cm^{-2} at 1.55 V. The current density at the same potential increases to almost 30 mA cm^{-2} after 1000 CV, and this value is maintained for 3000 CV. Then the activity starts to decrease, but it keeps high values of activity during almost 5000 cycles, where it decreases until 10000 cycles where the activity is lost. A restructuration of the catalyst surface occurs during the first 30 cycles, due to the Ru-enrichment of the surface resulting in a very active catalytic surface.[16]

MEA Characterization

$NdMn_{1.5}Ru_{0.5}O_5$

Next, the OER activity and durability of $NdMn_{1.5}Ru_{0.5}O_5$ was measured in a PEMWE. The catalyst-coated membranes (CCMs) were prepared by the wet spraying technique using a vacuum heating table (Fuel Cell Store) to hold the Nafion 212 PEM substrate in place and heat it to 100 °C during catalyst deposition. The distance between spraying nozzle and substrate was kept at. 6 cm and the ink deposition rate was limited to 2–3 min mL^{-1}. The inks were prepared by mixing 10 mg of catalyst in 1 mL of ultra-pure H_2O (MiliQ, 18 MΩ cm^{-1}) and the desired amount of Nafion® D521 solution (5 wt.% in lower aliphatic alcohols and water) to achieve an ionomer content of 25 and 30 wt.% for the anode and cathode layers, respectively. The mixture was sonicated for at least 1 h until the catalyst was well dispersed. 1 mL of isopropanol (IPA, ACS reagent, ≥ 99.5%) was added and the mixture was sonicated for 10 min to reach the adequate dispersion and homogeneity of the ink. This process was scaled up to the desired volume of ink. Subsequent to spraying and drying, the CCM was hot pressed at 5 Mpa and 125 °C. The result is a CCM with $NdMn_{1.5}Ru_{0.5}O_5$ (0.5 mg_{Ru} cm^{-2}) at the anode and Pt/C 40% (0.4 mg_{Pt} cm^{-2}) at the cathode. The CCMs were tested in a PEMWE setup optimized for screening cell components. On both the anode and cathode sides, a Ti porous sintered layer (PSL) on Ti mesh (PSL/mesh-PTL) compound porous transport layer (PTL) produced by diffusion bonding coated with Pt was deployed [17]. On the cathode, a carbon paper sheet (Spectracarb 2050A-1050) was used as an additional layer contacting the cathode catalyst layer on one side, and the PTL on the other side. On both the anode and cathode sides Ti bipolar plates (Ti-BPPs) were employed. The cell-active area was 4 cm^2 and tests were carried out at 80 °C and ambient pressure. The polarization curves were measured galvanostatically according to the JRC EU-harmonized procedure employing a dwell and consecutive recording period of 10 s for each current step. PEMWE polarization curves up to 0.5 A cm^{-2} and durability tests at constant current density of 0.5 A cm^{-2} were recorded.
Catalyst-coated membranes with $NdMn_{1.5}Ru_{0.5}O_5$ as the anode catalyst and low Ru loadings of 0.5 mg_{Ru} cm^{-2} were produced by spray coating and subsequently tested in a PEMWE single cell with an active area of 4 cm^2. Figure 3a shows the polarization curve recorded up to 0.5 A cm^{-2} at 80 °C and 1 bar. The PEMWE with $NdMn_{1.5}Ru_{0.5}O_5$ anode achieves 1.97 V at 0.5 A cm^{-2}. Although the performance achieved is slightly higher than that of other catalysts, it should be noted that the cell denotes a performance within

the state of the art of other Ru-based catalysts but with a ruthenium loading one order of magnitude lower than the usual reported anodes. [18,19].

Durability tests in single-cell configuration were conducted at constant current density. The cell was maintained at a current density of 0.5 A cm^{-2} during 100 h and a polarization curve was performed up to 0.5 A cm^{-2} at the end of the test to compare the performance with the initial one. Figure 4a shows an E_{cell} of 1.99 V at the end of the durability test denoting a degradation rate of only 200 µV h^{-1} of the cell. Such degradation is lower than that of other Ru-based catalysts, but very similar to that reported for Ir-based [21], or Ir-Ru-mixed catalysts [22].

Figure 3b shows cell potential throughout the durability test. It can be observed that although the cell manifests an initial activation process, after a few hours the potential stabilizes and remains constant throughout the test. Further on, towards the half the test a shutdown was carried out. The cell recovers performance almost immediately, giving an indication of the stability offered by the catalyst.

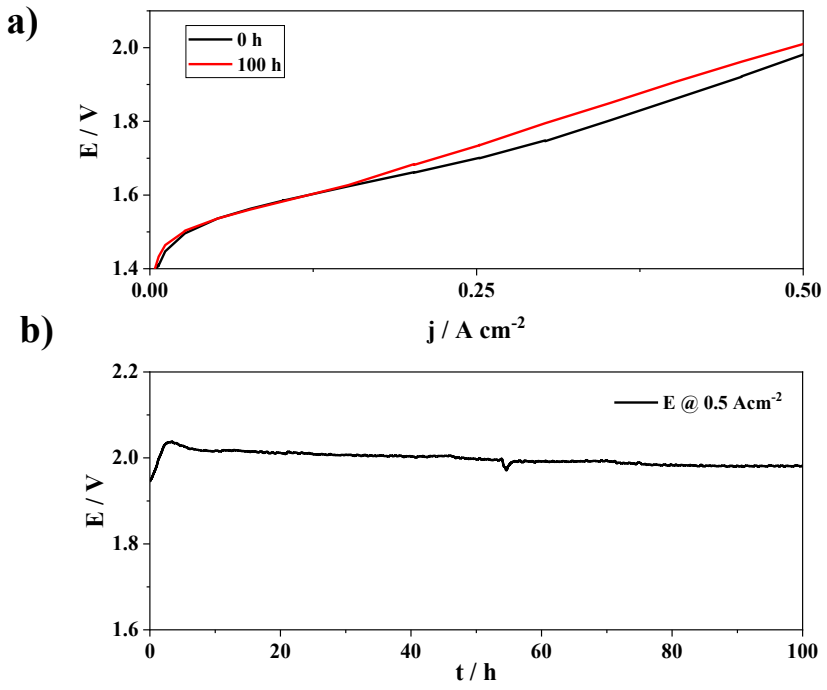

Figure 3 a) Polarization curve up to 0.5 A cm^{-2} before (black) and after (red) and b) cell potential constant current density 0.5 A cm^{-2} during 100 h for PEM electrolyzer based in 0.4 mg_{Pt} cm^{-2} as cathode and 0.5 mgRu cm^{-2} as anode obtained at 80 °C and 1 bar with Nafion 212

CENmat (Cutting Edge nanomaterials) has taken the approach of finely dispersing the Iridium nanoparticles on a support to increase the mass activity or Iridium, in turn reducing the amount of the Iridium needed for PEMWE. We herein present the summary report of all the developed catalysts and updated information on upscaling.

1.1.2 Synthesis and characterization: CENmat

All the synthesis routes chosen are wet chemical synthesis routes for the ease of scalability and reproducibility.

Novel Catalyst: OXYGN-A

A transition metal oxide support was used to synthesize this catalyst owing to its conductivity and stability in harsh acidic OER regime. OXYGN-A-0 was synthesized and thoroughly characterized both electrochemically and physio-chemically.

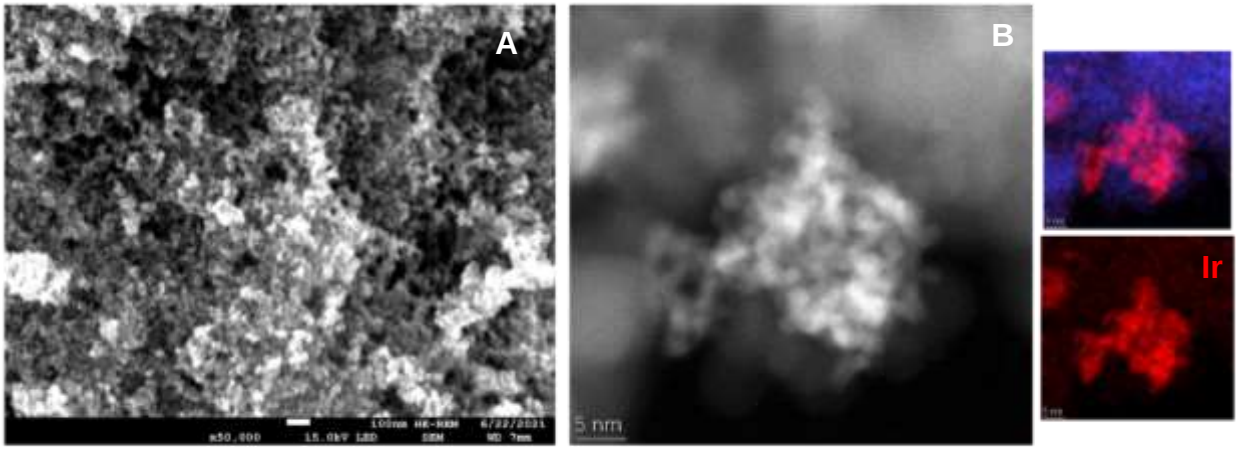

Figure 4 (A) SEM image of as synthesized catalyst (B) TEM image and HAADF of the OXYGN-A-0

From the SEM image (figure 4A) we can see the microscopic morphological features of the newly developed catalyst. The Ir dispersion on support looks to be in small nano aggregates form resulting in the less catalyst surface area. In TEM/HAADF image (figure 4B) we can see Iridium dispersed on the support, however clustering of Iridium can be observed.
To understand better the active area available in the prepared catalyst for the catalysis BET surface area was evaluated. OXYGN-A-0 found to have 41.5 m^2g^{-1} of surface area compared to 30 m^2g^{-1} commercial IrO_2.
As synthesized catalyst was thoroughly characterized in a 3-electrode cell set up. For electrochemical characterization details of experiments please refer D1.3.

Electrochemical measurement protocol consists of three sequences, a cyclic voltammetry within the voltage range 0.05-1.45 V, with a sweep rate 50 mV s^{-1} for three cycles to eradicate the influence of oxidation of impurities in oxidation current. In sequence LSVs were performed for three cycles within the voltage range 1.2-1.7 V with scan rate of 10 mV s^{-1}. All the results shown are iR corrected. This protocol will be same for all developed catalysts.

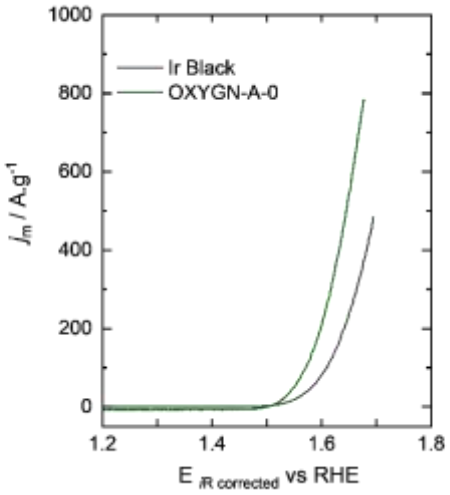

Figure 5 Mass specific OER activity comparison on Ir Black and OXYGN-A-0

Figure 5 shows mass normalised LSV curve for the OER catalysts. As shown that onset potential as well as mass specific OER activity of the synthesized catalysts were found to be better than that of Ir Black. These results show that the amount of noble metal can be reduced without affecting the OER activity.

3 grams of OXYGN-A-0 was synthesized as sent to partner FZJ for single cell evaluation. However, the single cell test performed at Julich did not reach the project target of 1.9V@2Acm^{-2} with 0.2 $mg_{Ir}cm^{-2}$ of Iridium loading with this catalyst as can be seen in the figure 6.

To engineer a catalyst that works in a system; partner CENmat decided to come up with another supported Iridium catalyst. From now on we will refer to this catalyst as OXYGN-A-1.

As we can see (figure 6A) that newly synthesized OXYGN A-1 outperforms the Iridium black in the whole potential range. At 1.6 V vs RHE the mass normalised activity of OXYGN-A-1 is approximately 3 times that of Iridium Black (figure 6B).

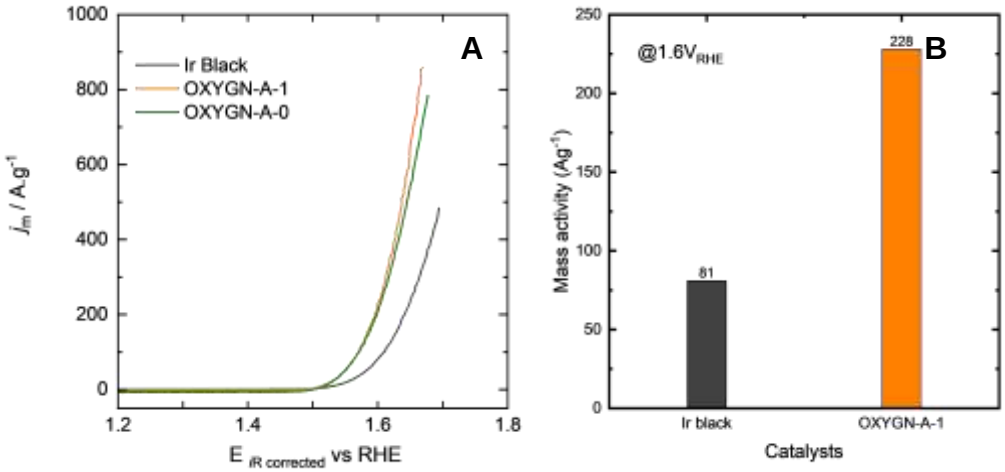

Figure 6 Mass specific OER activity comparison

As synthesized catalyst was characterized with SEM to understand the dispersion of Iridium nanoparticles on support. As seen in the SEM images (figure 7) whitish Iridium is dispersed on grayish support. The Iridium nanoparticles can be seen in aggregates and clusters. However, these clusters are very homogeneously distributed. To understand the oxidation state of Iridium in the as synthesized catalysts XPS measurements were performed.

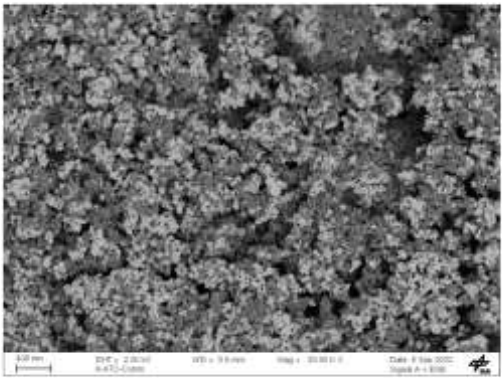

Figure 7 SEM image od OXYGN-A-1 catalyst.

3 g as synthesized catalyst was delivered to FZJ for single cell testing.

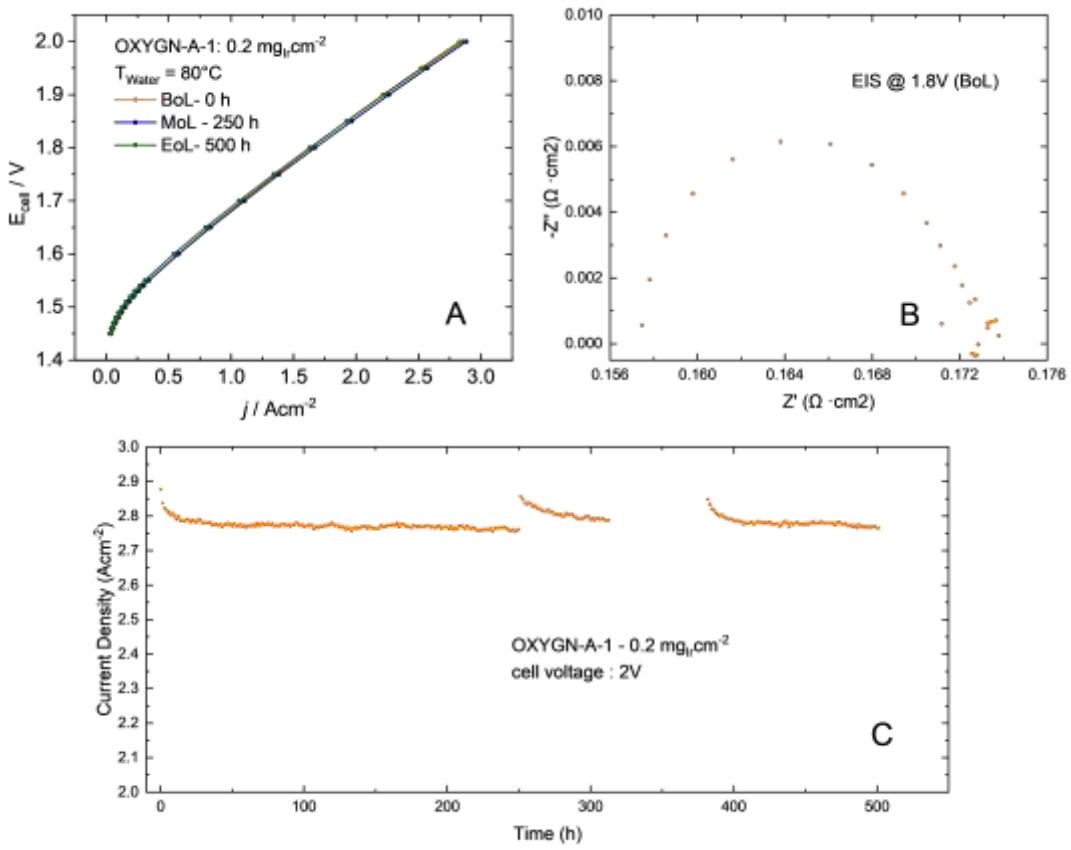

Figure 8 (A) Polarization curves (B) BoL EIS curve at 1.8 V (C) Potentistatic durability curve for 500 h at 2V (all tested at FZJ)

As you can see in figure 8A, the BoL polarization curve (orange curve), where *the cell has achieved 2.8 Acm^{-2} of current density at 2V at Iridium loading of 0.2 mg$_{Ir}$cm^{-2}. At 1.9V the cell surpasses the project target (2 Acm^{-2} at 1.9V) and achieves 2.21 Acm^{-2}.* The cell durability (figure 8C) was tested in potentiostatic mode at 2V for 500 hours and cell was found to be very stable and no degradation was recorded. The EoL polarization curve (Figure 6A, green curve) also shows that the cell performance was very stable, and no catalyst degradation was observed. Based on this performance OXYGN-A-1 was chosen (refer D1.4) to be used in stacks (both benchmark and final stack).

To ensure sustainability of synthesis process 2 more and different synthesis routes were developed by choosing a greener solvent namely OXYGN-A-2 & OXYGN-A-3. We also aimed to better disperse the Iridium nanoparticles on support with the newly developed synthesis routes. To firmly anchor the Iridium nanoparticles on support heat treatment of as synthesized catalyst were also explore. The solid lines represent the OER activity of as synthesized catalysts, and the dashed line represents the OER activity of the catalyst after heat treatment.

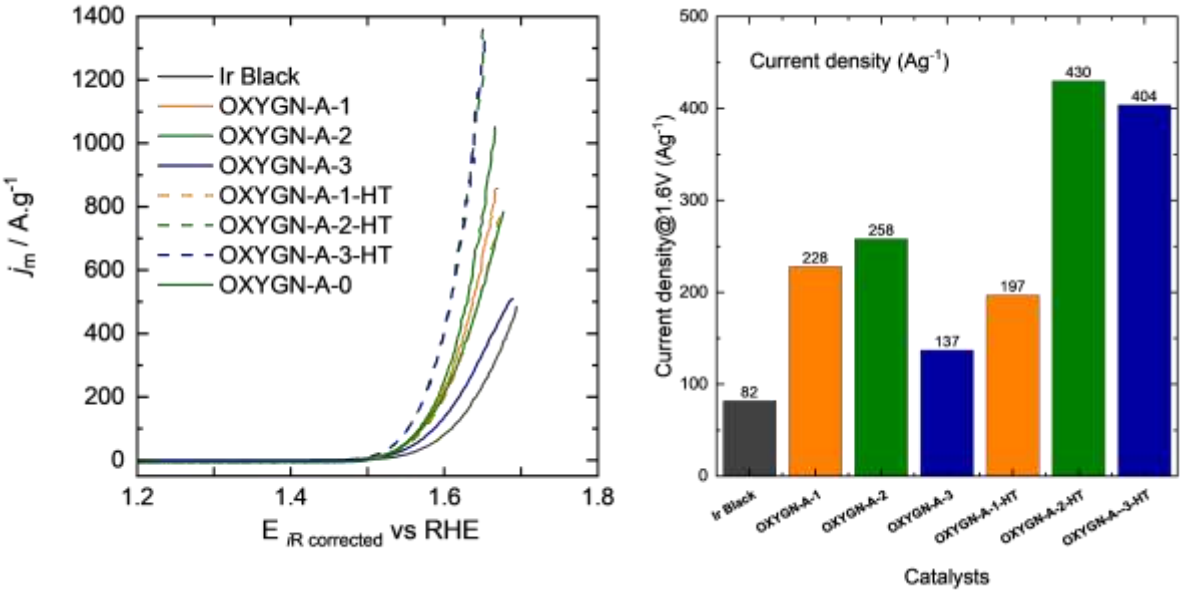

Figure 9 (A) Mass specific comparison of OER activity of synthesized catalysts (B) Mass normalised current density at 1.6 V of catalysts.

Figure 9A shows mass normalised OER activity of catalysts. All as synthesized catalysts outperforms the commercial Ir black over the whole potential range. After heat treatment the OER activity of OXYGN-A-1 catalyst remains almost the same while for OXYGN-A2&3 the OER activity was significantly increased after heat treatment. Mass normalised current density of all the tested catalysts was compared with Iridium black at1.6V (figure 9B). All the as synthesized as well as heat treated catalysts have better mass normalised oxygen evolution activity compared to benchmarked Ir black.

Novel Catalyst OXYGN-M

In the next stage of the PROMET-H2 project. Learning from our previous experience one dimensional support was chosen to help form an Iridium network with anode catalyst layer by the virtue of catalyst itself. From now on we will refer this catalyst as OXYGN-M. figure 10A, shows the cyclic voltammetry comparison of OXYGN-M to Ir black. From the characteristic peaks in hydrogen underpotential deposition region (below 0.3 V) dispersed Iridium on support has the same characteristics as metallic Iridium. The mass normalised OER activity of OXYGN-M is much superior compared to Iridium black. At 1.55 V the mass normalised current density is 88 and 17.8 Ag-1 for OXYGN-M and Ir black respectively (figure 10B). Looking at the kinetic parameter of tafel slope of it can also be seen that OXYGN-M has better kinetics than Iridium black (figure 10C). Catalyst was then galvanostatically at 10mAcm-2 in 3 electrode system for 30k seconds and was found to be stable (figure 10D).

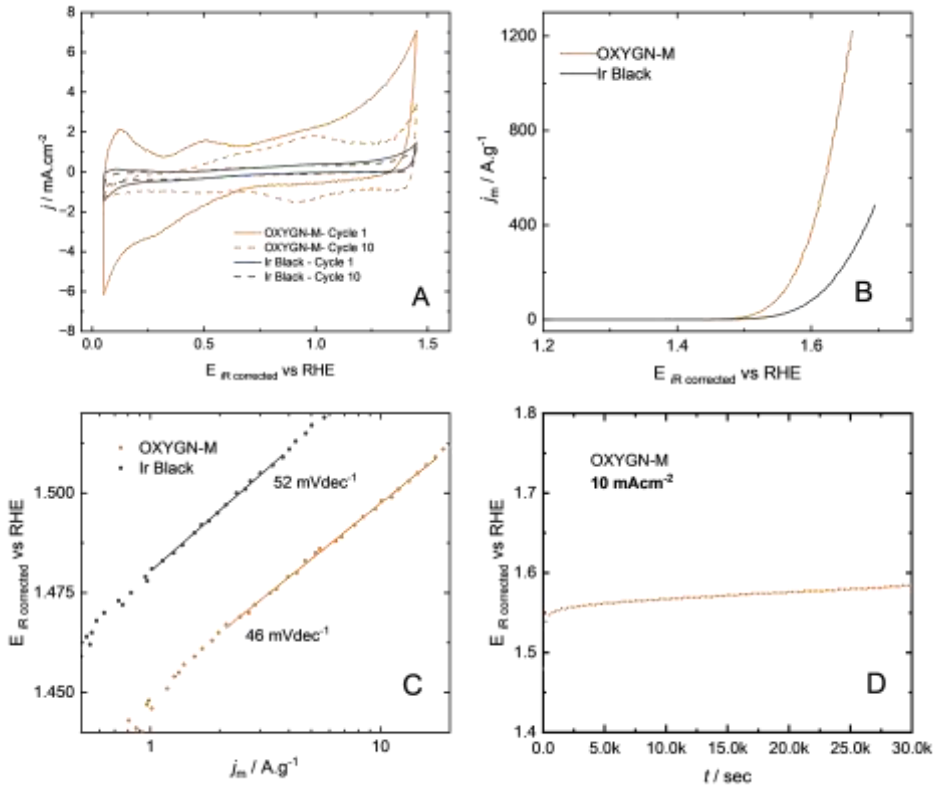

Figure 10 (A) Cyclic voltammetry (B) Mass specific (C) OER activity of OXYGN-M with Ir black (D) chronopotentiometry @ 10mAcm-2 of OXYGN-M

To screen the catalyst in the real-world scenario, CENmat has tested the catalyst in single cell by CENmat and DLR. The single cell test was run for 2000 h (figure 11A, orange line) in CENmat in galvanostatic mode (constant current 2Acm-2) where the global degradation rate in found to be only 15 micro volt per hour. To validate the results the catalyst was sent to partner FZJ to make the CCM with 0.2 $mg_{Ir}cm^{-2}$ and a single cell was tested for 1000 hours (constant current 2Acm-2) at DLR (figure 11A, green line).

When we look at the BoL and EoL on (CENmat tested single cell), polarization curve (figure 11B) we see that at lower current densities the HFR at EoL is lower than the beginning of life. EIS spectra at 0.2 Acm^{-2}, also confirms the same observation (figure 11C).

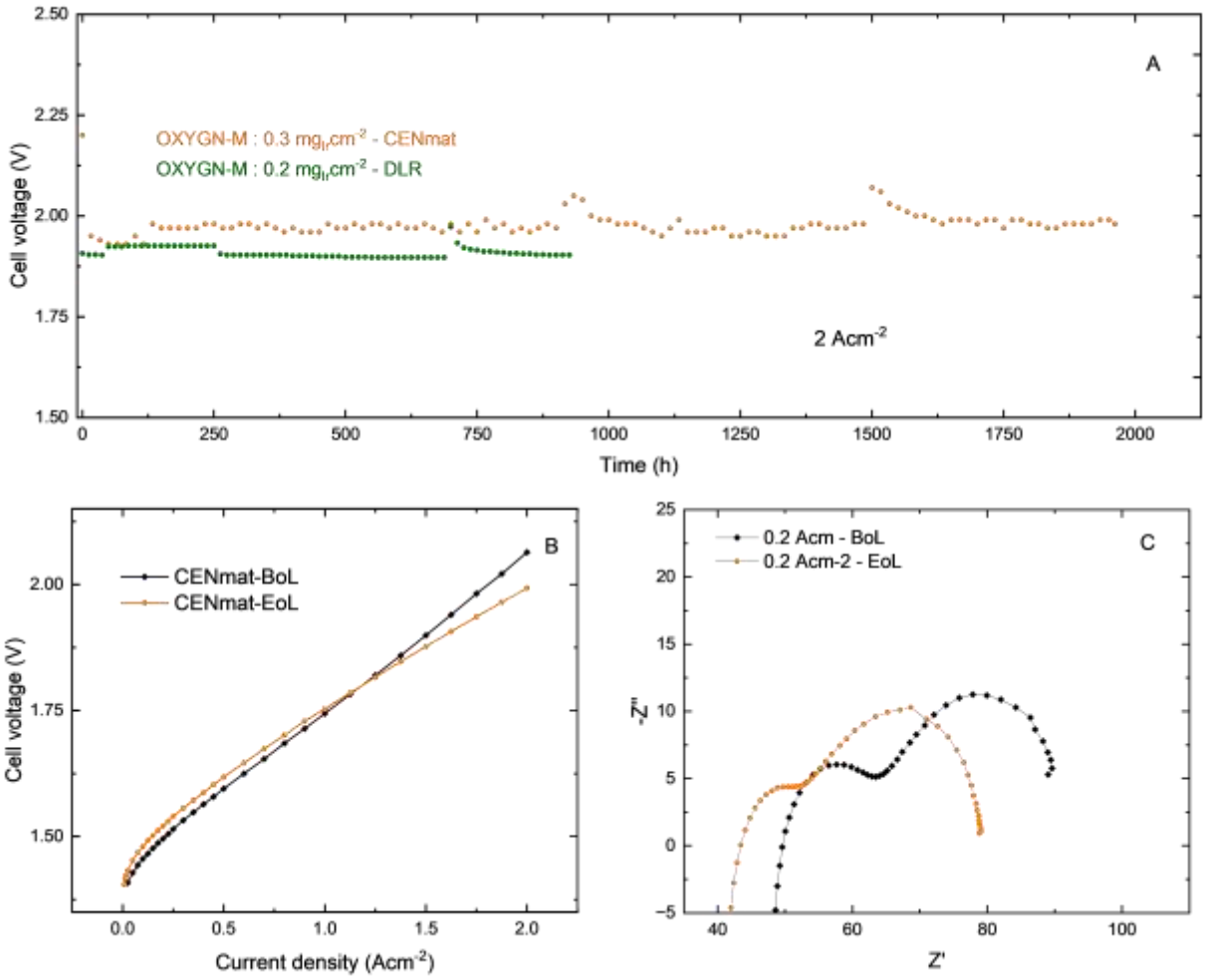

Figure 11 (A) Single cell durability tests in CENmat and DLR (B) Bol and EoL polarization curve for CENmat single cell test (C) Bol and EoL EIS for CENmat single cell test

Extensive SEM characterization were performed on pristine and CENmat operated Anode catalyst layer to help understand the anode catalyst layer evolution during operation. As we can see in the pristine (figure 12 A,C) as the one dimensional morphology of support has remain intact the CCM fabrication process. However, interestingly in 2000h operated anode catalyst layer (figure 12 B,D), the support's one dimensional morphology has diminished and a very porous architecture of anode catalyst layer has emerged which is solely made of network of spherical aggregates of nanoparticles. This also shows that the support has leached out and the whole anode catalyst layer goes through a in situ restructuring.

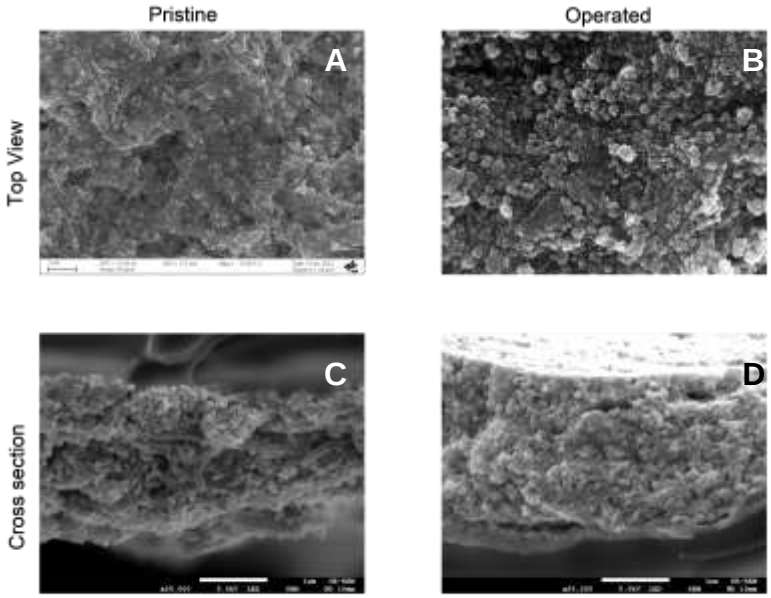

Figure 12 (A-B) Top view (C-D) cross section of pristine and CENmat operated membrane.

We also characterized the pristine and operated CCMs with AFM. Looking at height profile (figure 13 A, C) we can clearly see the ionomer distribution and one-dimensional support morphology in pristine CCM but an entangled web like structure in the operated CCM. Nano-electrical electron flux ((figure 13 B, D) has a huge difference in pristine and operated membrane. That might be because of leaching or restructuring of support where ionomer associated with the support also leaches away or restructures.

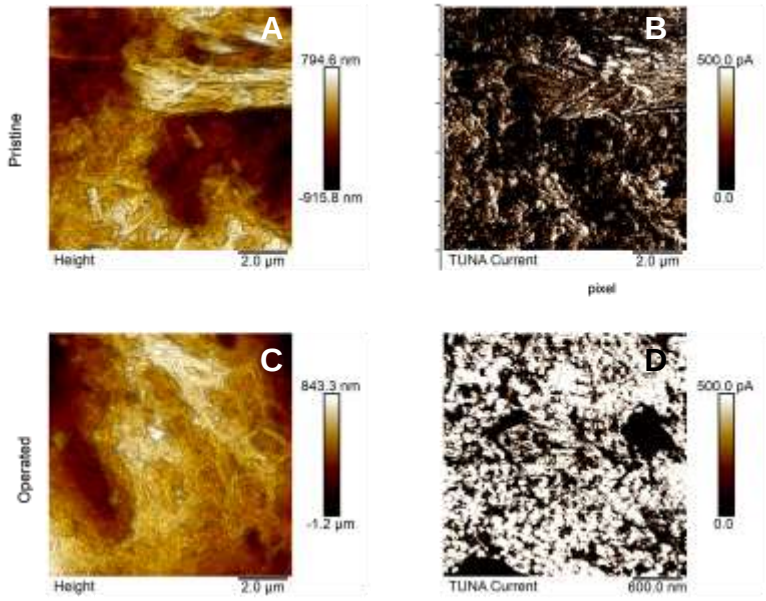

Figure 13 (A,C) Height distribution and TUNA current (B,D) pristine and CENmat operated membrane.

1.2 Hydrogen Evolution Reaction (HER)

CENmat has followed similar strategy of using a support material to reduce the Platinum loading on the cathode side of PEMWE was followed. However, the support chosen here is a functional support which is active towards the hydrogen evolution reaction itself to provide the assistance to platinum.

1.2.1 Synthesis and characterization

CENmat has prepared a very low loading HYGEN-M-1 catalyst for facilitating hydrogen evolution reaction. With HYGEN-M-2 amount of Platinum loading on support was increased. The catalyst was prepared via a wet chemical synthesis route for the ease of scalability in the later stages of the project.

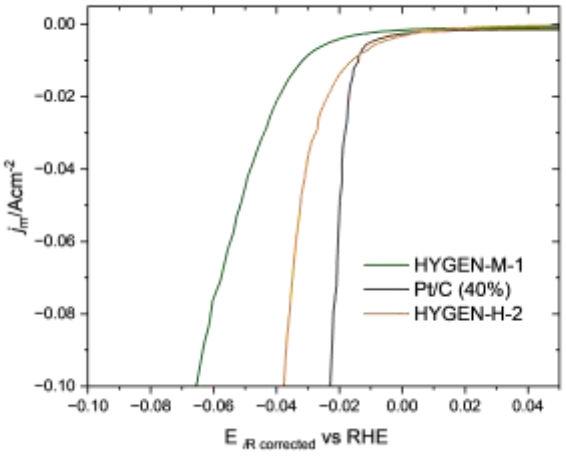

Figure 14 Comparison of HER activity of as synthesized catalyst with commercial Pt/C (40 wt.%)

Figure14 shows area (geometric) normalised LSV curve for the HER catalysts. As can be seen specific current density newly developed HYGEN-M-2 has been found to have comparable HER activity to commercial Pt@C (40 wt.%) at 10mA cm^{-2}. These results show that the amount of noble metal can be reduced without affecting the HER activity in RDE measurements. Long term testing is going on at CENmat to analyze the stability of as synthesized catalyst.
3 grams of this catalyst was sent to WP2 partner FZJ for testing in single cell. Single cell performance (figure 17) was found to be 2V @ approximate 1A cm^{-2} with 0.98 mg_{Pt} loading on cathode catalyst layer. Obtained performance is much lower than the project target of 1.9 V @2A cm^{-2}.

1.3 Upscaling: Updated information

CSIC: Sr_2CaIrO_6

*CSIC´*s catalysts were not selected as the candidates for the large scale electrolyzer. However, in view of the outstanding performance of Sr_2CaIrO_6, published in the frame of the project in the articles D. Galyamin et al. *Nature Commun. (2023) 14:2010* and J. Torrero et al. A*dvanced Energy Materials (2023) 2204169;* the catalyst was optimized and scaled up following different strategies.

1) We removed the high pressure of oxygen needed for the synthesis of the catalyst. The novel catalyst prepared without pressure of oxygen present similar catalytic performance as the one requiring pressure.
2) A material using ball milling synthesis was prepared. By this technique we were able to reduce the particle size of the catalyst and therefore improve its intrinsic activity
3) Also, an acid leaching was performed in all the Sr_2CaIrO_6 catalysts to avoid the leaching of cations during the electrolyzer testing.

CENmat: OXYGN-A & OXYGN-M

As previously reported that OXYGN-A-1 was chosen based on single cell performance and durability to be the catalyst deployed in in 25kW electrolyser. Before single cell testing the developed material did undergo various upscaling steps from 100 mg to 6 grams batches which accounts for 60 times I crease in upscaling in catalyst. For upscaling of the catalyst materials, the focus was also on the proper synthesis conditions in order to mimic the same condition on the small scale. This becomes important especially in the case of nanomaterial production to avoid aggregations leading to strongly bonded colloidal particles which can not be broken down easily to nanometer size as opposed to agglomerates. Thus, strategies to avoid aggregation such as varying the a) precursors and b) reducing agents, or optimization of the solvents and temperature distribution within the reaction container etc. are developed. To ensure the that the upscaled materials are of same quality in performance samples of each batch of materials undergo the testing protocols in three electrode set-up to analyse their OER activity (figure 15) and was found out that all the batches have same mass specific activity for OER. Recently this synthesis has been upscaled up to 12 grams.

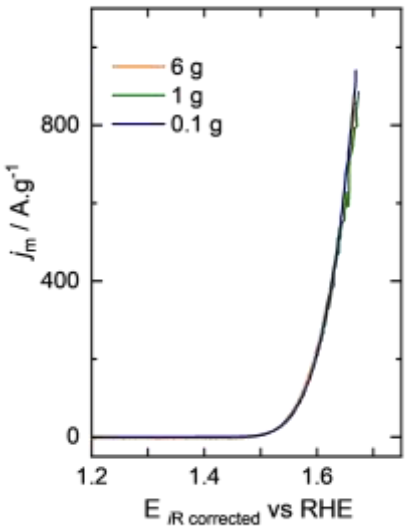

Figure 15 OER activity of upscaled catalyst of OXYGN-A-1

2 CRM free catalysts

2.1 Oxygen Evolution reaction (OER)

Minimization of high-cost metal electrocatalyst is necessary to achieve cost-effective green hydrogen production by proton exchange membrane (PEM) water electrolysis (WE). The large increase of the cost of Ir recently observed requires individuating alternative catalyst solutions for the oxygen evolution reaction (OER) in PEMWE. The OER is the rate determining step of the electrolysis process requiring high-cost noble metals with significantly high loading. A non-platinum group metal (non-PGM) anode catalyst based on silver and titanium suboxide was prepared and used for the oxygen evolution reaction in a PEMWE cell. By using a solid-state synthesis procedure, a silver nitrate and titanium suboxides (Ti_nO_{2n-1}) with Magneli phase powders were mixed and subjected thereafter to a thermal treatment at 300°C in a 50% H_2/N_2 gas stream to promote the inclusion of silver within the Ti-suboxides structure.

2.1.1 Synthesis and Characterization : CNR

For the oxygen evolution reaction (OER), an Ag-titanium suboxides catalyst was synthetized by a solid-state procedure. A silver nitrate precursor was supplied by Carlo Erba. Titanium suboxides powder (Ti_nO_{2n-1}) with Magneli phase, was prepared from a commercial titanium (IV) chloride solution ($TiCl_4$, Aldrich) by complexation of Ti ions and successive decomposition of the complex to form an amorphous oxide; this was subsequently reduced by a thermal treatment (1050 °C) with diluted hydrogen. $AgNO_3$ and Ti_nO_{2n-1}were mechanically mixed in the molar ratio of 30:70 in a porcelain mortar and ball milled in a planetary mill for 12 h/300 rpm to obtain an Ag/Ti-suboxides mixture. This Ag/Ti-suboxides-based catalyst was subjected to a thermal treatment at 300°C/1h in a tubular quartz reactor fed with a 50% H_2/N_2 gas stream to promote the inclusion of silver within the Ti-suboxides.

Physico-chemical and morphological properties of the catalysts were studied by X – ray diffraction (XRD), scanning electron microscopy (SEM) and X- ray photoelectron spectroscopy (XPS) before and post operation analyses. A Bruker D2 PHASER desktop diffractometer, operating at 40 kV and 20 mA, was used for investigating the structural properties of the catalysts. The measurements were conducted in a Bragg-Brentano geometry with a scan rate of 0.5° 2Θ min^{-1}. The diffraction patterns were analysed through the Joint Committee on Powder Diffraction Standards (JCPDS). SEM analyses were carried out by means of a FEI S – FEG XL30 microscope coupled with an energy dispersive X-ray spectrometer (EDX), operating at 25 kV before and after the steady-state operation (1000 h) and voltage cycles (24 h) tests. The anode surface composition was studied by using a Physical Electronics (PHI) 5800 – 01 spectrometer before and after durability and cycle tests as well.

The synthesis of the Ag/Ti-suboxides catalyst includes a first step related to the formation of titanium suboxides. This involves formation of an amorphous oxide phase with a subsequent reduction at 1050°C. Fig. 16 shows the SEM - EDX analyses of the obtained Ti-suboxides. No relevant amounts of impurities that may derive from the precursors are detected. Structural and physico-chemical characterizations (see below) have confirmed the presence of the Ti_nO_{2n-1}formulation with Magneli phase. In particular, the observed Ti/O at. ratio 0.82 (Fig. 16) is in good agreement with the general sub-oxide

formulation Ti_nO_{2n-1}that is indicative of the presence of specific oxygen vacancies. The achievement of a proper purity for the TiOx support with a Magneli phase structure containing a proper amount of oxygen vacancies represents one of the main challenges in the preparation of this anode catalyst. In the second step of catalyst preparation, the Ag precursor is mechanically mixed with Ti-suboxides. Thereafter the catalyst powder is subjected to a thermal treatment at 300 °C for 1 h with a 50% H_2/N_2 gas stream to promote the inclusion of silver within the Ti-suboxides structure.

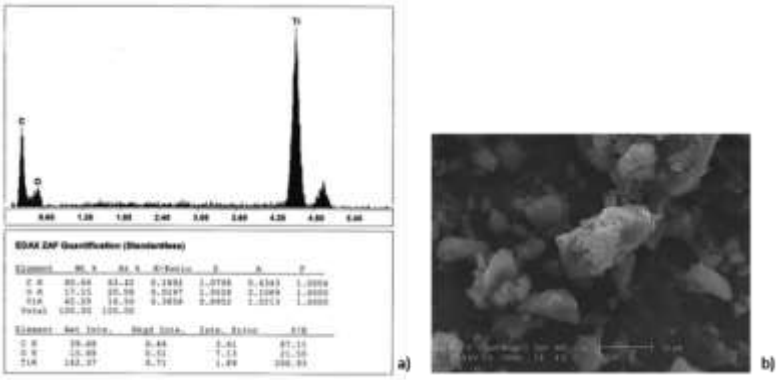

Figure 16 EDX a) and SEM b) analysis of the Ti- suboxides

SEM-EDX analysis showed no relevant impurities (Fig. 16). The composition after the reduction treatment was of 30:70 at. % Ag/Ti-suboxides.

An XRD pattern of the Ag/Ti-suboxides anode catalyst subjected to the thermal treatment at 300°C/1h with H_2 and N_2 (50:50%) is reported in Fig. 17. After a preliminary investigation of the thermal treatment up to 500 °C, a reduction treatment at 300 °C was selected to favour the inclusion of silver with the Ti-suboxides, while avoiding excessive sintering of catalyst particles. The $AgNO_3$ precursor was reduced to Ag nanoparticles during such treatment. The main diffraction peaks at 38° and 44° 2 theta were assigned to the 111 and 200 reflections of metallic Ag with face-centered cubic crystallographic structure (JCPDS: 04-0783). A crystallite size of 46 nm was determined from the Debye-Scherrer equation. The typical peaks of Ti_nO_{2n-1} (with n varying from 4 to 10) Magneli phase structure, after the thermal treatment, are evident especially for the phases characterised by n = 4, 5 and 6. The inset shows the SEM image of the catalyst, a good dispersion of Ag on the Ti-suboxides is observed.

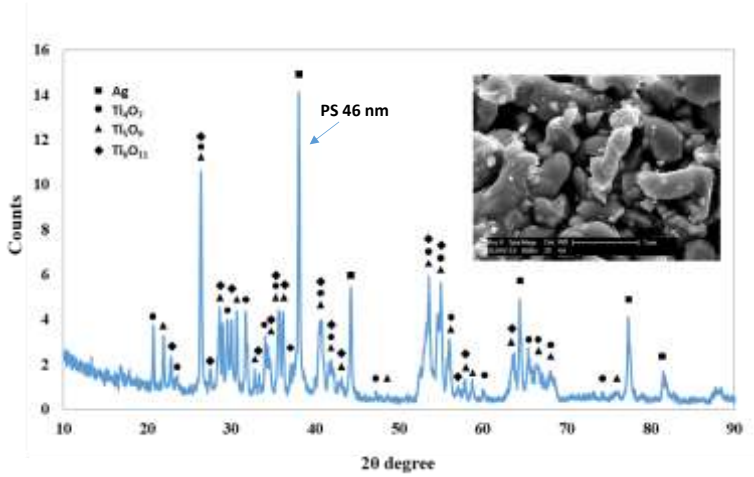

Figure 17 X-ray diffraction patterns of the Ag/Ti-suboxides anode catalyst (JCPDS cards no. 04-0783 (Ag), 1527759 (Ti_4O_7), 1520779 (Ti_5O_9), 1008201 (Ti_6O_{11}); inset: SEM image of the Ag/Ti-suboxides catalyst.

Ex-situ post-operation analyses were carried out on the BoL MEA and used MEA (electrochemical test reported in D2.6), in order to understand the catalyst degradation or any change on the anode catalyst oxidation state that could have occurred during the voltage cycle test. The XRD patterns of the Ag/Ti-suboxides anode catalyst and membrane of the used MEA are reported in Fig. 17. There was a lower evidence of metallic Ag in the used anode, scraped from the MEA, essentially the Ti-suboxides were present. No change in crystallite size for Ti_4O_7, Ti_5O_9 and Ti_6O_{11} based-Ti-suboxides before and after test was oberved (Figs. 16 and 18a). The XRD pattern of the used membrane is reported in the Fig. 18b. The peaks of the metallic Ag were evidently present in the membrane pattern. This means that the metallic Ag migrated inside the membrane or Ag particles sticked better to the membrane than the Ti-suboxide support during operation. As well known, the XRD analysis gives information about the bulk structure where no particular change of the Ag based-anode catalyst oxidation state was observed. A reduction of crystallite size for the metallic Ag was observed after the durability test, from 46 nm at BoL to 25.3 nm at the end of life (EoL) (Figs 16 and 18b).

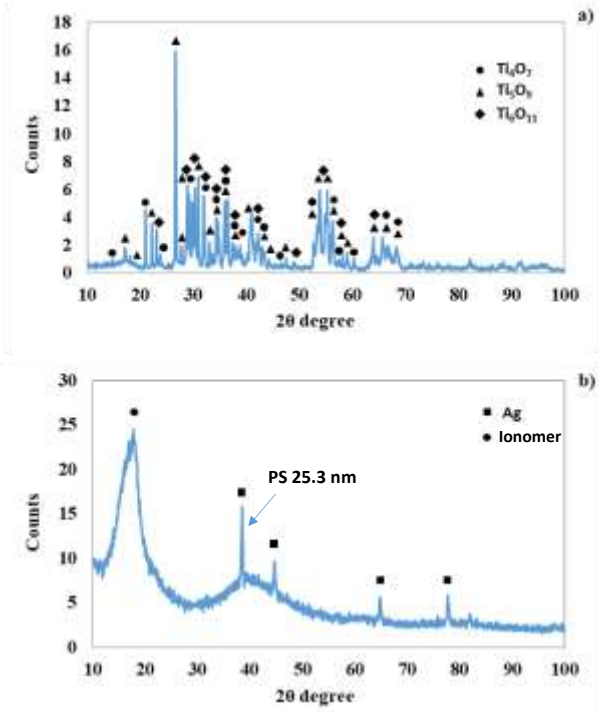

Figure 18 X-ray diffraction patterns of a) Ag/Ti-suboxides catalyst scraped from the MEA and b) Nafion N212 membrane after the stability and cycle test

A morphology investigation of the Ag/Ti-suboxides anode, scraped from a fresh MEA, and the MEA after the voltage cycling test (electrochemical test reported in D2.6) are shown in Fig. 19. The SEM analysis (Fig. 19a-19c) showed for the Ag/Ti-suboxides-based fresh anode the occurrence of mixture of nanosized irregularly shaped and faceted particle agglomerates formed of fine particles (≤ 10 μm), associated to the Ti-suboxides. The Ag particles were more evident in Fig. 19b and 19c, at higher magnifications with agglomerates smaller than a few hundred micrometres. In the BoL sample, the presence of the ionomer was evident, whereas in the used sample the ionomer was less observed (Fig. 22a-22c vs. Fig. 19d-19f). A decrease of the atomic ratio F/Ti was recorded by SEM-EDX. No significant change in morphology with the durability test (Fig. 19d-19f) was observed, just a sintering of metallic Ag in the used sample compared to the fresh samples in contrast the observation by X-ray diffraction (Fig. 18b).

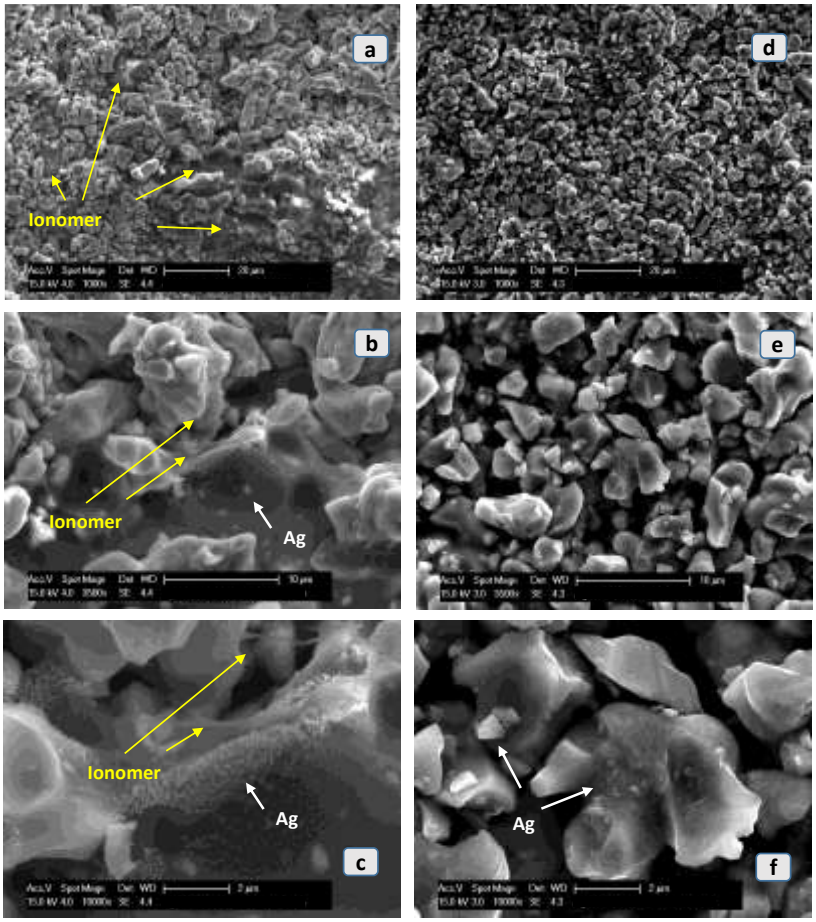

Figure 19 SEM for Ag/Ti-suboxides anode catalyst before (a, b, c) and after (d, e, f) durability and duty

High resolution XPS analyses were carried out on the anodic surface of a fresh MEA and used MEA subjected to durability and duty cycles; Ag3d and Ti2p photoelectron lines were selected for the assessment of Ag and Ti oxidation states (Fig. 20a, 20b). By comparing the B.E. of Ag3d peaks, a shift to lower B.E. in the used sample was evident (Fig. 20a) and this was related to an oxidation of the Ag^0 to Ag^+ for the used anode-based MEA. The B.E. shifted from 367.97 eV in the fresh catalyst to 367.18 eV in the used catalyst. It is worth mentioning that in the case of silver, formation of oxidised Ag from metallic Ag is usually accompanied by a negative shift of the B.E. contrary to what occurs with most of the metals.

The high resolution spectra of Ti2p before and after the durability and duty cycles test are reported in Fig. 20b. In this case a shift at higher B.E. was observed for the used sample indicating an oxidation of the Ti surface. The shift indicated a partial modification of sub-stoichiometric Ti-suboxides species on the anode surface that produced a higher oxidised phase. The reoxidation of Ti suboxides to form TiO_2 on the surface under electrolysis conditions may have an impact on both series and polarisation resistance being this part of a catalyst-ionomer composite network that extends the reaction zone from the catalyst-membrane interface to the catalytic layer.

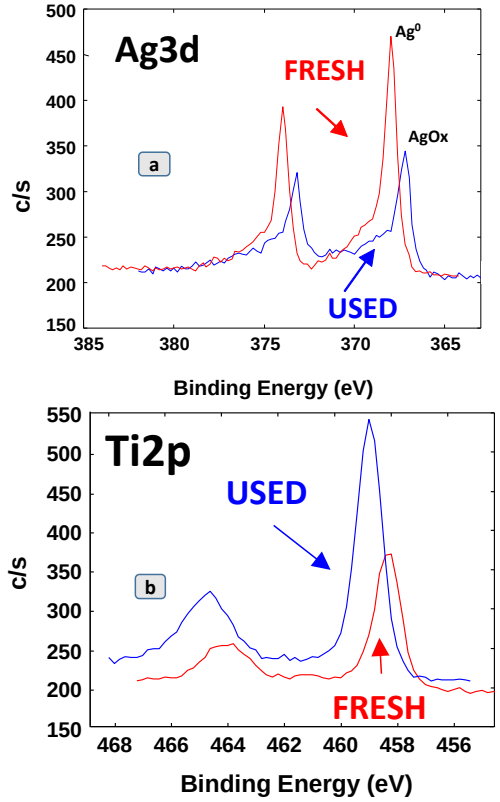

Figure 20 XPS for Ag/Ti-suboxides anode catalyst before and after durability and duty cycles

To summarise, XPS analysis has clearly indicated an oxidation of the Ti-suboxides on the surface. However, this does not cause any dramatic performance loss during 1000 h steady state operation under electrolysis conditions, or increase of series and polarisation resistance or increase of the slope of polarisation curves at high current density. Thus, it is speculated that some breaks in the TiO_2 oxide surface layers may occur at high potentials allowing an electronic percolation eventually by a tunnelling effect as it occurs with Ti bipolar plates in conventional PEM electrolysis stacks. This would suggest that the growth of the TiO_2 oxide layer remains confined to the surface in the present Ti sub-oxides and electronic percolation possibly occurs through alternative mechanisms. Our electrochemical and physicochemical results seem to confirm such aspects. In particular, the surface oxidation of the sub-oxides detected by XPS was not observed in the XRD analysis of the anode support after the durability study. This indicates that the bulk characteristics are not significantly changed.

Considering the recent dramatic increase in the Ir cost, this work aims at finding an anodic formulation alternative to iridium-based anode catalysts. The large increase of Ir cost appears mainly related to the insufficient reserves to manage all potential applications including PEM electrolysis fed by renewable power sources. This is a well consolidated technology to produce green hydrogen. The limited Ir reserves could thus limit PEM electrolysis in contributing significantly to the installation of the required electrolysis plans, in the order of tens of GW, as planned in several countries. The risks associated to the high cost and availability of iridium clearly indicate the need to explore alternative solutions.

In this regard, the present activity provides a study of a non-PGM anode catalyst for PEM electrolysis applications. A solid-state procedure was used to obtain Ag/Ti-suboxides, from silver nitrate and titanium suboxides with Magneli phase. The thermal reduction process promoted the inclusion of silver within the Ti-suboxides.

Post operation analysis showed some catalyst agglomeration and migration of silver onto the membrane which was indicative of lower interaction with the TiOx phase. An increase of the oxidation states for Ag and Ti was also observed. However, such modifications did not produce relevant performance losses. In general, there is still a good possibility of improving catalyst properties in terms of dispersion, particle size and interface with the solid polymer electrolyte in a PEM electrolysis cell.

Thus, the developed Ag/TiOx catalyst effectively requires some improvements before becoming a satisfactory replacement for the IrOx benchmark. Our activity was essentially addressed to provide a basis for an alternative catalyst formulation that could undergo to successive amelioration. As mentioned above, the required improvements regard the achievement of a mesoporous catalyst morphology, a decrease of the particle size, a better inclusion of Ag in the Ti suboxide structure etc.

3 Reference

[1] A.V. Morozkin, Y.D. Seropegin, Sm–Ru–Ge system at 1070 K, J. Alloys Compd. 365 (2004) 168–172. https://doi.org/10.1016/S0925-8388(03)00652-2.

[2] D. Huang, S. Liu, H. Xu, Y. Du, Phase equilibria of the Mg–Mn–Zn system at 593 K (320 °C), J. Alloys Compd. 688 (2016) 1115–1124. https://doi.org/10.1016/j.jallcom.2016.07.120.

[3] C. de la Calle, J.A. Alonso, M.J. Martínez-Lope, M. Retuerto, M. García-Hernández, M.T. Fernández-Díaz, Ru–Ru Metal–Metal Bonding in the Chains of Edge-Sharing Octahedra of NdMn 1.5 Ru 0.5 O 5 : A Neutron Powder Diffraction and Magnetic Study, Eur. J. Inorg. Chem. 2010 (2010) 781–789. https://doi.org/10.1002/ejic.200900626.

[4] R.D. Shannon, Revised effective ionic radii and systematic studies of interatomic distances in halides and chalcogenides, Acta Crystallogr. Sect. A. 32 (1976) 751–767. https://doi.org/10.1107/S0567739476001551.

[5] C.C.L.L. McCrory, S. Jung, J.C. Peters, T.F. Jaramillo, Benchmarking heterogeneous electrocatalysts for the oxygen evolution reaction, J. Am. Chem. Soc. 135 (2013) 16977–16987. https://doi.org/10.1021/ja407115p.

[6] M. Retuerto, L. Pascual, F. Calle-Vallejo, P. Ferrer, D. Gianolio, A.G. Pereira, Á. García, J. Torrero, M.T. Fernández-Díaz, P. Bencok, M.A. Peña, J.L.G. Fierro, S. Rojas, Na-doped ruthenium perovskite electrocatalysts with improved oxygen evolution activity and durability in acidic media, Nat. Commun. 10 (2019) 2041. https://doi.org/10.1038/s41467-019-09791-w.

[7] I. Rodríguez-García, D. Galyamin, L. Pascual, P. Ferrer, M.A. Peña, D. Grinter, G. Held, M. Abdel Salam, M. Mokhtar, K. Narasimharao, M. Retuerto, S. Rojas, Enhanced stability of SrRuO3 mixed oxide via monovalent doping in Sr1-xKxRuO3 for the oxygen evolution reaction, J. Power Sources. 521 (2022) 230950. https://doi.org/10.1016/j.jpowsour.2021.230950.

[8] X. Miao, L. Zhang, L. Wu, Z. Hu, L. Shi, S. Zhou, Quadruple perovskite ruthenate as a highly efficient catalyst for acidic water oxidation, Nat. Commun. 10 (2019) 1–7. https://doi.org/10.1038/s41467-019-11789-3.

[9] J. Kim, P. Shih, Y. Qin, Z. Al-Bardan, C. Sun, H. Yang, A Porous Pyrochlore Y 2 [Ru 1.6 Y 0.4]O 7– δ Electrocatalyst for Enhanced Performance towards the Oxygen Evolution Reaction in Acidic Media, Angew. Chemie Int. Ed. 57 (2018) 13877–13881. https://doi.org/10.1002/anie.201808825.

[10] N. Zhang, C. Wang, J. Chen, C. Hu, J. Ma, X. Deng, B. Qiu, L. Cai, Y. Xiong, Y. Chai, Metal Substitution Steering Electron Correlations in Pyrochlore Ruthenates for Efficient Acidic Water Oxidation, ACS Nano. 15 (2021) 8537–8548. https://doi.org/10.1021/acsnano.1c00266.

[11] M.A. Hubert, A.M. Patel, A. Gallo, Y. Liu, E. Valle, M. Ben-Naim, J. Sanchez, D. Sokaras, R. Sinclair, J.K. Nørskov, L.A. King, M. Bajdich, T.F. Jaramillo, Acidic Oxygen Evolution Reaction Activity-Stability Relationships in Ru-Based Pyrochlores, ACS Catal. (2020) 12182–12196. https://doi.org/10.1021/acscatal.0c02252.

[12] D. Galyamin, J. Torrero, I. Rodríguez, M.J. Kolb, P. Ferrer, L. Pascual, M.A. Salam, D. Gianolio, V. Celorrio, M. Mokhtar, D. Garcia Sanchez, A.S. Gago, K.A. Friedrich, M.A. Peña, J.A. Alonso, F. Calle-Vallejo, M. Retuerto, S. Rojas, Active and durable R2MnRuO7 pyrochlores with low Ru content for acidic oxygen evolution, Nat. Commun. 14 (2023) 2010. https://doi.org/10.1038/s41467-023-37665-9.

[13] Y. Lin, Z. Tian, L. Zhang, J. Ma, Z. Jiang, B.J. Deibert, R. Ge, L. Chen, Chromium-ruthenium oxide solid solution electrocatalyst for highly efficient oxygen evolution reaction in acidic media, Nat. Commun. 10 (2019). https://doi.org/10.1038/s41467-018-08144-3.

[14] S. Hao, M. Liu, J. Pan, X. Liu, X. Tan, N. Xu, Y. He, L. Lei, X. Zhang, Dopants fixation of Ruthenium for boosting acidic oxygen evolution stability and activity, Nat. Commun. 11 (2020) 5368.

https://doi.org/10.1038/s41467-020-19212-y.
[15] C. Lin, J.-L. Li, X. Li, S. Yang, W. Luo, Y. Zhang, S.-H. Kim, D.-H. Kim, S.S. Shinde, Y.-F. Li, Z.-P. Liu, Z. Jiang, J.-H. Lee, In-situ reconstructed Ru atom array on α-MnO2 with enhanced performance for acidic water oxidation, Nat. Catal. 4 (2021) 1012–1023. https://doi.org/10.1038/s41929-021-00703-0.
[16] J.Y. Kim, J. Choi, H.Y. Kim, E. Hwang, H.J. Kim, S.H. Ahn, S.K. Kim, Activity and stability of the oxygen evolution reaction on electrodeposited Ru and its thermal oxides, Appl. Surf. Sci. 359 (2015) 227–235. https://doi.org/10.1016/J.APSUSC.2015.10.082.
[17] S. Stiber, H. Balzer, A. Wierhake, F.J. Wirkert, J. Roth, U. Rost, M. Brodmann, J.K. Lee, A. Bazylak, W. Waiblinger, A.S. Gago, K.A. Friedrich, Porous Transport Layers for Proton Exchange Membrane Electrolysis Under Extreme Conditions of Current Density, Temperature, and Pressure, Adv. Energy Mater. 11 (2021) 2100630. https://doi.org/10.1002/aenm.202100630.
[18] S. Song, H. Zhang, X. Ma, Z. Shao, R.T. Baker, B. Yi, Electrochemical investigation of electrocatalysts for the oxygen evolution reaction in PEM water electrolyzers, Int. J. Hydrogen Energy. 33 (2008) 4955–4961. https://doi.org/10.1016/j.ijhydene.2008.06.039.
[19] J. Cheng, H. Zhang, G. Chen, Y. Zhang, Study of IrxRu1−xO2 oxides as anodic electrocatalysts for solid polymer electrolyte water electrolysis, Electrochim. Acta. 54 (2009) 6250–6256. https://doi.org/10.1016/j.electacta.2009.05.090.
[20] Q. Feng, Z. Zhao, X.-Z. Yuan, H. Li, H. Wang, Oxygen vacancy engineering of yttrium ruthenate pyrochlores as an efficient oxygen catalyst for both proton exchange membrane water electrolyzers and rechargeable zinc-air batteries, Appl. Catal. B Environ. 260 (2020) 118176. https://doi.org/10.1016/j.apcatb.2019.118176.
[21] G. Li, H. Yu, D. Yang, J. Chi, X. Wang, S. Sun, Z. Shao, B. Yi, Iridium-Tin oxide solid-solution nanocatalysts with enhanced activity and stability for oxygen evolution, J. Power Sources. 325 (2016) 15–24. https://doi.org/10.1016/j.jpowsour.2016.06.004.
[22] G. Jiang, H. Yu, J. Hao, J. Chi, Z. Fan, D. Yao, B. Qin, Z. Shao, An effective oxygen electrode based on Ir0.6Sn0.4O2 for PEM water electrolyzers, J. Energy Chem. 39 (2019) 23–28. https://doi.org/10.1016/j.jechem.2019.01.011.

Acknowledgement

This project has received funding from the European Union's Horizon 2020 research and innovation programme under grant agreement No 862253".